

30 Mar 2001, 1:30 pm - 3:30 pm

## An Experimental Study of Seismic Bearing Capacity of Shallow Footings

Awad A. Al-Karni  
*King Saud University, Saudi Arabia*

Muniram Budhu  
*University of Arizona, Tucson, AZ*

Follow this and additional works at: <https://scholarsmine.mst.edu/icrageesd>



Part of the [Geotechnical Engineering Commons](#)

### Recommended Citation

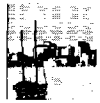
Al-Karni, Awad A. and Budhu, Muniram, "An Experimental Study of Seismic Bearing Capacity of Shallow Footings" (2001). *International Conferences on Recent Advances in Geotechnical Earthquake Engineering and Soil Dynamics*. 1.

<https://scholarsmine.mst.edu/icrageesd/04icrageesd/session09/1>



This work is licensed under a [Creative Commons Attribution-Noncommercial-No Derivative Works 4.0 License](#).

This Article - Conference proceedings is brought to you for free and open access by Scholars' Mine. It has been accepted for inclusion in International Conferences on Recent Advances in Geotechnical Earthquake Engineering and Soil Dynamics by an authorized administrator of Scholars' Mine. This work is protected by U. S. Copyright Law. Unauthorized use including reproduction for redistribution requires the permission of the copyright holder. For more information, please contact [scholarsmine@mst.edu](mailto:scholarsmine@mst.edu).



## **AN EXPERIMENTAL STUDY OF SEISMIC BEARING CAPACITY OF SHALLOW FOOTINGS**

**Awad A. Al-Karni**  
King Saud University  
Department of Civil Engineering  
P.O. Box 800, Riyadh, 11421, Saudi Arabia

**Muniram Budhu**  
University of Arizona  
Department of Civil Engineering and Engineering Mechanics  
Tucson, AZ 85721, USA

### **ABSTRACT**

In this paper, the results of an experimental investigation on the response of model shallow footings to horizontal accelerations are presented. The experiments were conducted on square and rectangular footings resting on or embedded in a dry sand and shaken in a shake box. The shake box was designed to subject the soil to simple shear conditions during shaking. Model footings, constructed from lead, were used to study the seismic bearing capacity. The influence of the magnitude and frequency of the horizontal accelerations, the static bearing capacity safety factor, the footing shape, the depth of embedment, and the relative density of the soil on the seismic bearing capacity were investigated. It is shown that the initial shear fluidization acceleration is the maximum acceleration sustainable by a shallow footing regardless of the static bearing capacity safety factor. Critical accelerations from limit equilibrium analyses do not compare favorably with the experimental results except when the change in angle of friction from cyclic densification was taken into account.

### **KEYWORDS**

Bearing capacity, shallow, foundation, footing, seismic, acceleration, cohesionless, soil

### **INTRODUCTION**

The design of foundations to support various dynamic loads has received considerable attention in recent years. These dynamic loads may come from earthquakes, nuclear detonations, blasting, pile driving, water waves, and machine vibrations. In comparison with the extensive studies on the static bearing capacity of shallow footings, only a limited amount of information is available in the literature on the dynamic bearing capacity of soils. Where the latter information is available, the analyses and experimental investigations deal essentially with vertical vibrations as in machine foundations (e.g. D'Appolonia et. al., 1968).

It has been reported in the literature (e.g. Seed and Lee, 1966) that many buildings have failed during earthquakes by soil bearing capacity failure. Most of these failures are attributed to soil liquefaction - a condition where the mean effective stress in a saturated soil, essentially loose saturated cohesionless soil, is reduced to zero by the development of large excess pore water pressures. For example, during the Niigata, Japan,

earthquake of June 1964, soil liquefaction caused the apartment buildings at Kawagishicho to tilt, some by as much as 60°, without structural damage. Relatively few cases of foundation failures in partially saturated (dense or loose) sands and dense saturated sands have been reported in the literature during seismic events. A few examples of failures in these types of deposits were reported by Watanabe (1966) and Okamoto (1984).

Selig and McKee (1961) investigated the behavior of many small footings resting on dense uniform Ottawa sand and subjected to vertical impulse loads and static loads. They observed the classical general shear failure in static load tests but local shear failure (associated with failure in loose sands) under dynamic loads. Large settlements (about 75% of the footing width) were reported for dynamic tests after the failure plane was developed.

Vesic et. al., (1965) studied experimentally the dynamic bearing capacity of strip footings on a sand under transient vertical loads. All tests were performed using a circular, rigid, rough plate, having a diameter of 101.6

mm and resting on the surface of homogeneous dense sand. The sand bed was prepared in a watertight steel box 127 cm square and 178 cm deep. They showed that the dynamic bearing capacity was about 30 percent lower than the static bearing capacity and suggested that the reduction in strength is equivalent to a decrease in the angle of internal friction of about 2 degrees. The effects of overburden pressures were not considered in this study.

Okamoto (1956) used a box, 15 cm width x 60 cm length x 30 cm depth, containing dense sand with angles of friction ranging from 38° to 50°, that was shaken horizontally on a shake table to determine the seismic bearing capacity of shallow footings. The footing was simulated by a rectangular test plate, 6.1 cm x 15.0 cm, and loaded vertically. Settlement of the footing was observed when a horizontal sinusoidal acceleration of amplitude 0.38g was applied for 1.3 seconds. When the test plate was loaded obliquely, it slid horizontally, due to shear failure of the soil, before settlement began. The bearing capacity was found to decrease linearly with increasing horizontal accelerations for both dry and saturated sand. These test results were compared with a theoretical solution (Okamoto, 1956) in which the resultant of the weight and the inertia forces of the footing was treated as an inclined load applied to the soil at an angle equal to  $\tan^{-1}(k_h)$  from the vertical axis where  $k_h$  is the horizontal acceleration coefficient. Good agreement between the theoretical and experimental results was reported. Inertia of the soil and surcharge loading were not considered in the theoretical solution.

Recently, several theoretical studies on the seismic bearing capacity of soils supporting shallow footings have been presented (Sarma and Issofelis, 1990; Richards et. al., 1991, Richards et. al., 1993; Budhu and Al-karni, 1993). These studies used a limit equilibrium analysis with various assumptions on the shape of the failure surface. Richards et. al. (1991) used a simple Coulomb type planar failure surface, while Sarma and Issofelis (1990), and Budhu and Al-karni (1993) used logarithmic spiral failure surfaces. The differences between the seismic bearing capacity calculated from these theories were presented by Budhu and Al-karni (1993). The intention of this contribution is to present laboratory test results on the performance of shallow footings under horizontal accelerations and to compare the experimental results with existing theoretical analyses.

## SEISMIC BEARING CAPACITY EQUATION

The seismic bearing capacity factors described by Budhu and Al-karni (1993) can be used to modify popular static bearing capacity equations (Terzaghi, 1943, Meyerhof, 1963, Hansen, 1970, Vesic, 1973). For

example, the Meyerhof bearing capacity equation for vertical load can be modified to become a general equation to include seismic effects as follows.

$$q_{uE} = CN_c s_c d_c e_c + q_f N_{qs} s_q d_q e_q + 0.5B\gamma N_{\gamma s} s_\gamma d_\gamma e_\gamma \quad (1)$$

where  $q_{uE}$  is the ultimate seismic bearing capacity,  $C$  is soil cohesion,  $N_{cs}$ ,  $N_{qs}$ ,  $N_{\gamma s}$ , are static bearing capacity factors,  $s$  and  $d$  are shape and depth factors respectively,  $q_f$  is the overburden pressure,  $B$  is the footing width,  $\gamma$  is the unit weight of the soil, and  $e_c$ ,  $e_q$ , and  $e_\gamma$  are the seismic factors calculated from Budhu and Al-karni (1993) as

$$e_c = \exp(-4.3k_h^{1+D}) \quad (2)$$

$$e_q = (1 - k_v) \exp\left[-\left(\frac{5.3k_h^{1.2}}{1 - k_v}\right)\right] \quad (3)$$

$$e_\gamma = \left(1 - \frac{2}{3}k_v\right) \exp\left[-\left(\frac{9k_h^{1.1}}{1 - k_v}\right)\right] \quad (4)$$

where  $k_h$  is the horizontal acceleration coefficient,  $k_v$  is the vertical acceleration coefficient,  $D = C/(\gamma H)$  and  $H$  is the depth of the failure zone from the ground surface given as

$$H = \frac{0.5B}{\cos\left(\frac{\pi}{4} + \frac{\phi}{2}\right)} \exp\left(\frac{\pi}{2} \tan \phi\right) + D_f \quad (5)$$

where  $D_f$  is the depth of the footing and  $\phi$  is the angle of friction of the soil.

## DESIGN OF MODEL FOOTING

One of the problems with dynamic laboratory tests is that scaling effects make the interpretation of the results for field application difficult. Equations that can be used to scale shake table models were developed by Iai (1989). The basic approach taken by Iai (1989) was followed to determine appropriate models for the shake box experiments. The ultimate seismic bearing capacity ( $q_{uE}$ ) of a square footing resting on the surface of a cohesionless soil ( $D_f = 0$ ) is obtained from equation (1) by setting  $C = 0$  and  $q_f = 0$ , resulting in

$$q_{uE} = 0.5B\gamma N_{\gamma s} s_\gamma d_\gamma e_\gamma \quad (6)$$

and the ultimate load ( $Q$ ) is

$$Q = 0.5B^3\gamma N_{\gamma E} s_\gamma d_\gamma \quad (7)$$

where  $N_{\gamma E} = N_{\gamma s} e_{\gamma}$ .

Since  $N_{\gamma E}$  is the dimensionless seismic bearing capacity factor,  $s_{\gamma}$  and  $d_{\gamma}$  are shape and depth factors respectively, then the relationship between the model and the prototype depends only on the width ( $B$ ) of the footing and the unit weight of the soil ( $\gamma$ ). By denoting the width scale by  $\lambda_B$  and the unit weight scale by  $\lambda_{\gamma}$ , the following relationships are obtained

$$B_p = \lambda_B B_m \quad (8a)$$

$$\gamma_p = \lambda_{\gamma} \gamma_m \quad (8b)$$

where the subscripts  $m$  and  $p$  denote model and prototype, respectively.

The unit weight scale ( $\lambda_{\gamma}$ ) is equal to one if the unit weight of the soil in the model and the prototype is the same. Consequently, the width scale ( $\lambda_B$ ) is the only scale to be considered in designing model footings in the shake box tests. By substituting equation (8a) into equation (7), the ultimate load on a prototype footing ( $Q_p$ ) equivalent to a model footing of width  $B_m$  is

$$Q_p = 0.5 \lambda_B^3 B_m^3 \gamma N_{\gamma E} s_{\gamma} d_{\gamma} \quad (9)$$

The equivalent load on the model footing is then

$$Q_m = \frac{Q_p}{\lambda_B^3} \quad (10)$$

The ultimate load ( $Q_p$ ) for a prototype square footing,  $B_p = 1$  m, resting on the surface of a cohesionless soil with  $\phi = 40^\circ$  is  $8.32 \times 10^5$  kN. This prototype footing can be represented by a model footing of width  $B_m = 10$  cm ( $\lambda_B = 10$ ) in which the ultimate load for the model footing ( $Q_m$ ) is 832.0 kN. Since the ultimate load depends on  $B_m^3$ , its magnitude increases significantly as the footing width increases.

For the shake box experiments, a low value of  $B_m$  was used to obtain a manageable footing weight and to minimize the footing height. The footings were fabricated from lead blocks, each of thickness 2.5 cm. By stacking and attaching these blocks, footings with different weights and safety factors can be obtained. A summary of the size and weight of two of the model footings to be discussed in this paper is shown in Table 1.

Two shapes - square and rectangular - of footings were used (Fig. 1). The following protocol was used to label the footings: the first letter represents the shape, S is square, R is rectangular; the two digit number is the width of the footing in centimeters to the nearest centimeter; F denotes the static bearing capacity safety

factor for a centric vertical load and the number following F is the value of the safety factor. For example, S10F3 is a square model footing of width 10.16cm (Table 1) designed with a static bearing capacity safety factor of 3.

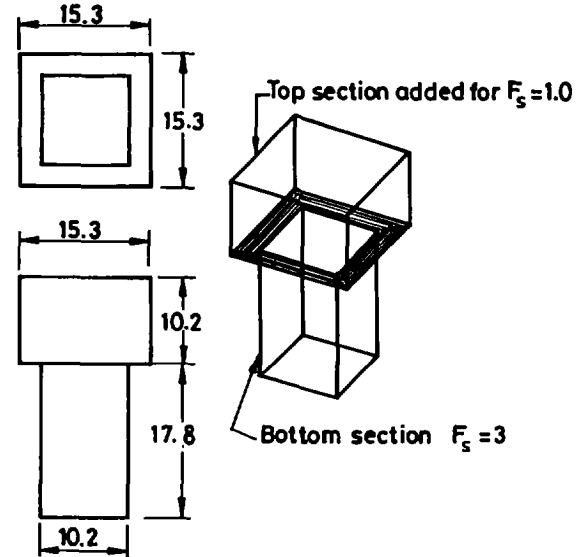


Fig. 1. Schematic diagram of the model footings constructed from lead.

Table 1. Summary of model footings

Model	Size (cm × cm × cm)	Weight (kg)
S10F1	10.16 × 10.16 × 28	62.7
S10F3	10.16 × 10.16 × 17.8	20.9

## SHAKE TABLE

A shake box (Fig. 2), 4.27m long, 1m wide, and 1.37m high with a test section or inner box (3.35m long × 0.94m wide × 0.94m high) and two end compartments (each 0.46m long) was used to conduct the test program. The shake box is composed of two boxes sharing the same longitudinal sides and base. The end walls of the outer box are fixed while the inner end walls are fitted with roller bearings to allow them to rotate to deform the sand mass from a rectangular to a parallelepiped configuration (simple shear) under a base acceleration. The compartments were used to collect sand during stopping and reversal of a sand spreader (see Al-Karni, 1993).

The longitudinal sides of the box were constructed from 2.54 cm thick plexiglass specially hardened and treated to reduce interface friction. The shaker box is supported on rollers running on steel I-beams fixed to the laboratory floor and displaced horizontally by an MTS actuator and control system. The range of horizontal displacement that could be applied was +7.65cm to -

7.65cm and the range of frequencies was 1 - 1000 Hz. Only horizontal acceleration can be applied to the shake box in the present design. Thus, in this paper, the generic term acceleration is used to denote horizontal acceleration.

### PROPERTIES OF SAND AND TEST PROCEDURE

A sand spreader was used to pluviate, in each pass, a thin layer of clean, dry, uniform silica #30 sand into the test box. The thickness, 6mm - 25mm, of the layer depended on the travel speed of the sand spreader. By controlling the openings on a perforated bar and the speed of the sand spreader, different void ratios of the sand could be obtained in the test box. A series of tests was performed on the sand according to ASTM procedures. The following are the relevant results: mean grain size 0.55mm; coefficient of uniformity,  $C_u = 2.5$ ; minimum void ratio,  $e_{min} = 0.58$ ; maximum void ratio,  $e_{max} = 0.95$ ; specific gravity,  $G_s = 2.64$ . Simple shear tests were conducted on the sand to determine the angle of friction at low stress levels (2 - 7 kPa). The results at different relative densities are shown in Fig. 3. Unless

otherwise stated, the relative density of the sand bed used in the experiments is  $67 \pm 5\%$ .

A model footing was placed on top of or embedded into the sand mass depending on the type of test desired. Three accelerometers were placed along a vertical line through the middle of the sand layer. One was affixed to the base of the shake box, and the other two were located at the top and mid-section of the sand bed. Two displacement sensors (linear variable displacement transducers, LVDT) were attached to the top of the footing, one at each end, and held in position by a stiff bar affixed to the top I beams of the shake box.

An initial series of tests was carried out to obtain the cyclic horizontal displacements and appropriate frequencies to be applied to the shake box for any desired acceleration. Measurements of the accelerations at the three positions stated above showed an amplification (ratio of acceleration at top of box to the acceleration at the base of the box) of the box of 1.11 (Fig. 4).

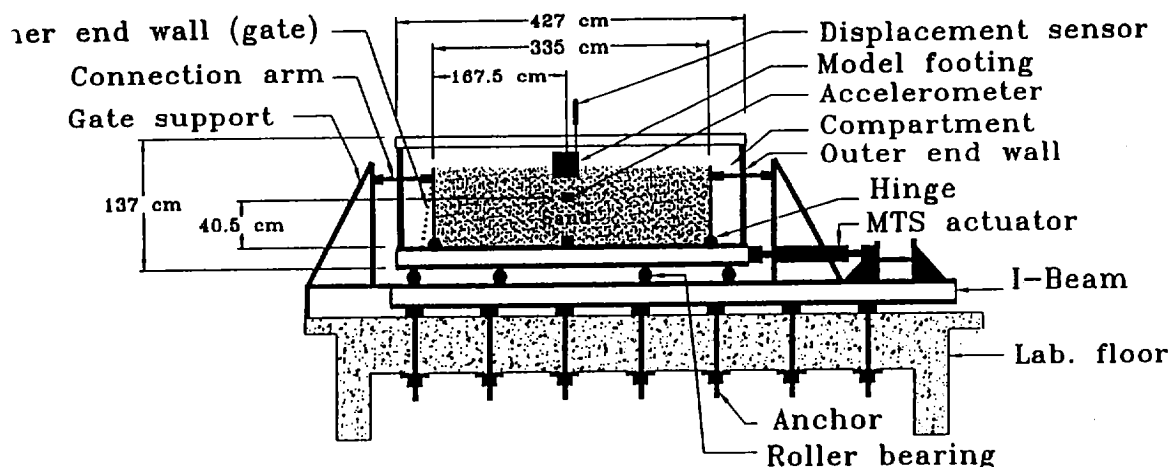


Fig. 2. Diagrammatic section of shake box and loading system.

### GENERAL TEST OBSERVATIONS

Model S10F3 was placed on top of the sand layer near the plexiglass side. The sand layer was shaken horizontally at different levels of accelerations at a frequency of 3 Hz. Each acceleration regime was ramped up to the desired level and kept there for about 25 seconds. A 12 second duration of a typical acceleration regime in which the desired acceleration amplitude was 0.6g is shown in Fig. 5a. For this regime, no movement of the footing was observed (Figs. 5b) for accelerations below 0.25g. Beyond this acceleration, for the next 3 seconds, the footing moved with a constant velocity of about 1.0 mm/sec as determined from the

slope of the displacement - time plot in Fig. 5b. At about 10 seconds (1 second of application of the peak acceleration of 0.6g), no further movement of the footing was recorded. One and a half second later, the stem of one of the LVDTs dropped out of its core and lodged on the surface of the sand. No further measurement of movements was possible. The stems of the LVDTs were each located at 5 mm from the edge of the footing. Thus, the footing tilted at least  $25^\circ$  suddenly. The test was continued by increasing the amplitude at each acceleration level at a frequency of 3Hz. The duration for each acceleration regime was 25 seconds. The test was stopped at maximum acceleration amplitude of 1.05g and the rotation and displacements

were then measured. The results revealed a tilt of  $55^\circ$ , a horizontal movement of about 60 mm and a vertical settlement of about 50 mm (Fig. 6).

A similar test was conducted using model S10F1. No movement occurred for accelerations less than 0.08g (Figs. 7a,b). After this acceleration, the footing settled at a rate of about 1.7 mm/sec and then suddenly tilted when the acceleration reached 0.15g.

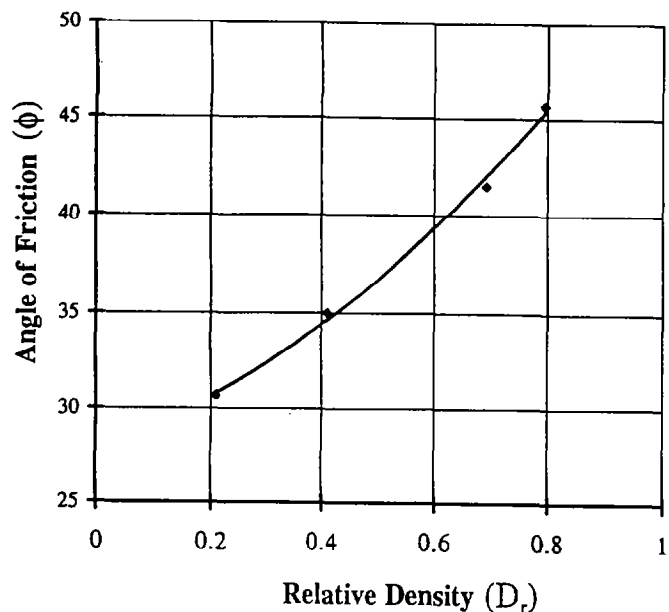


Fig. 3. The relationship between the relative density and the angle of friction for silica sand #30.

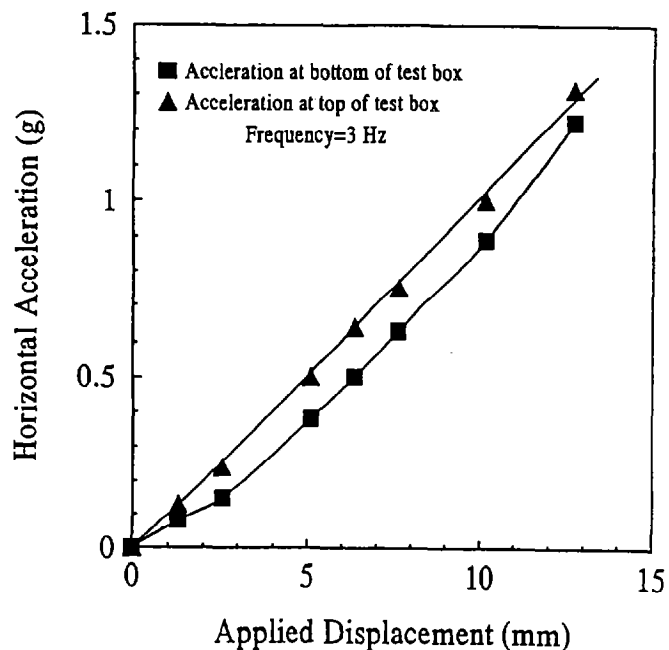
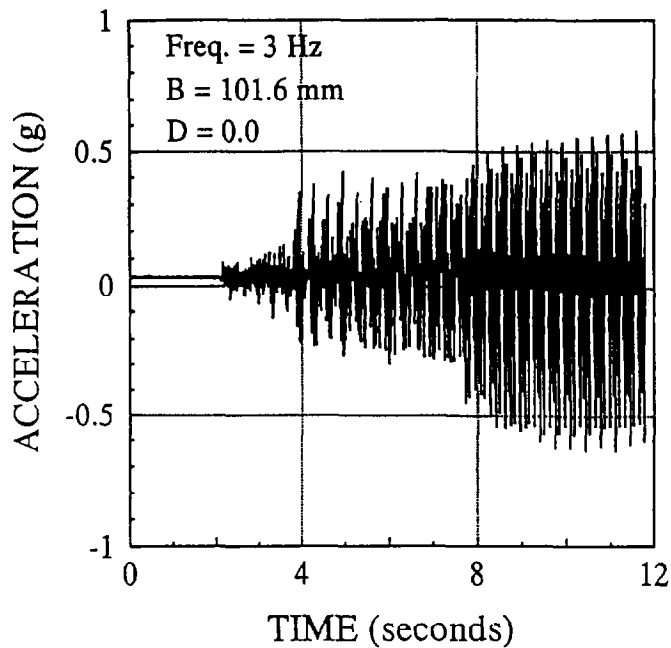
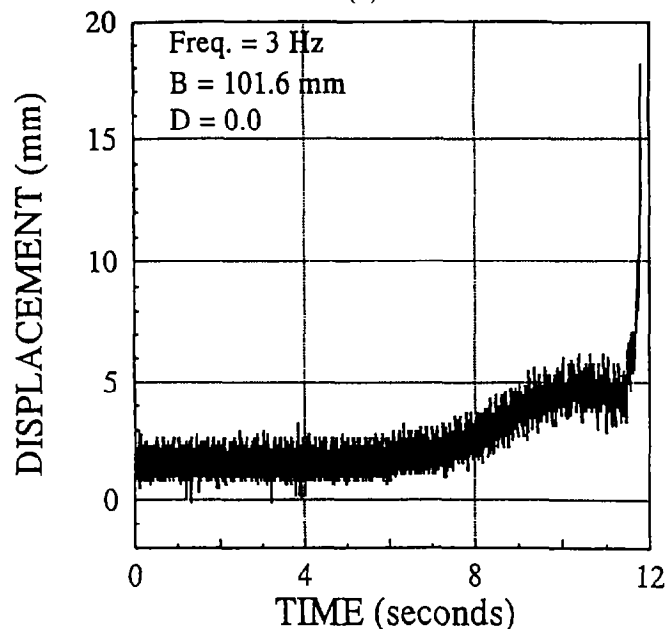


Fig. 4. The variation of acceleration with applied displacement at frequency of 3 Hz for the shake box.



(a)



(b)

Fig. 5. Model S10F3 (a) variation of acceleration with time (b) variation of displacement with time.

### SEISMIC FAILURE SURFACE

During the pluviation of the sand, it was observed that thin horizontal lines of dust were formed between the sand layers. Horizontal lines were drawn on the one of the plexiglass sidewalls to match the initial position of the lines of dust. After shaking, the current positions of the lines of dust in the sand bed were measured relative to their initial positions. Because of the unavailability of

X-ray facilities, this rather crude method only provided an approximate form of the failure surface.

In one of the tests to determine the seismic failure surface, the weight of model S10F1 was reduced to obtain a static factor of safety of 1.2 (S10F1.2) and this footing was placed on the surface of the sand bed prepared at a relative density of 41% (corresponding to  $\phi=35^\circ$ ). The footing was located near the plexiglass side wall of the shake box. Accelerations of 0.5g were applied at 3Hz for 75 seconds in an attempt to bring the footing to failure and to discern a failure surface.

The deformation pattern of the lines of dust beneath this model footing is shown in Fig. 8. Significant vertical movement of the sand layer was observed within a depth of 6 cm beneath the footing base. Plots of the variation of settlement with depth under the footing are shown in Fig. 8. Discerning a slip surface from Fig. 8 is difficult. Indeed, no clear failure or slip surface was detected in any of the tests conducted in this experimental program. A better experimental method (e.g. using x-rays with embedded lead markers) is required to determine the failure surface.

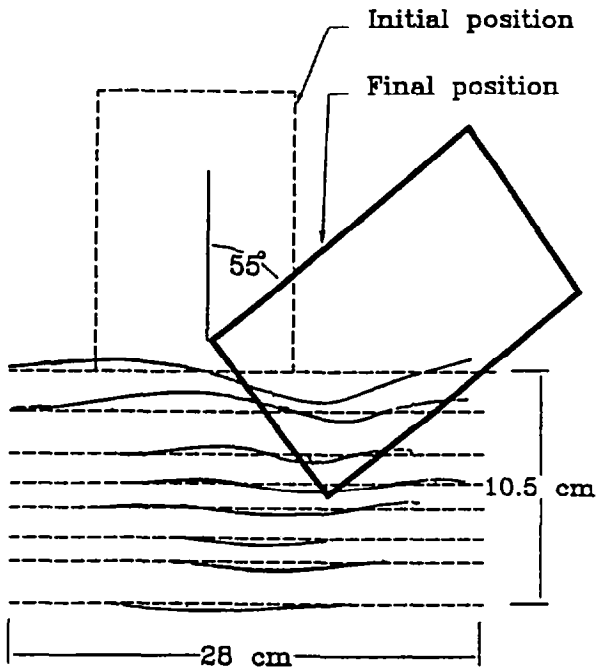


Fig. 6. Model S10F3 position before and after the sand bed was shaken at acceleration up to 1.05 g ( $\phi=41^\circ$ ).

### LOAD ECCENTRICITY

The eccentricity of loading and the corresponding calculated horizontal acceleration required to cause overturning is shown in Table 2. These eccentricities will not change the value of the critical acceleration as

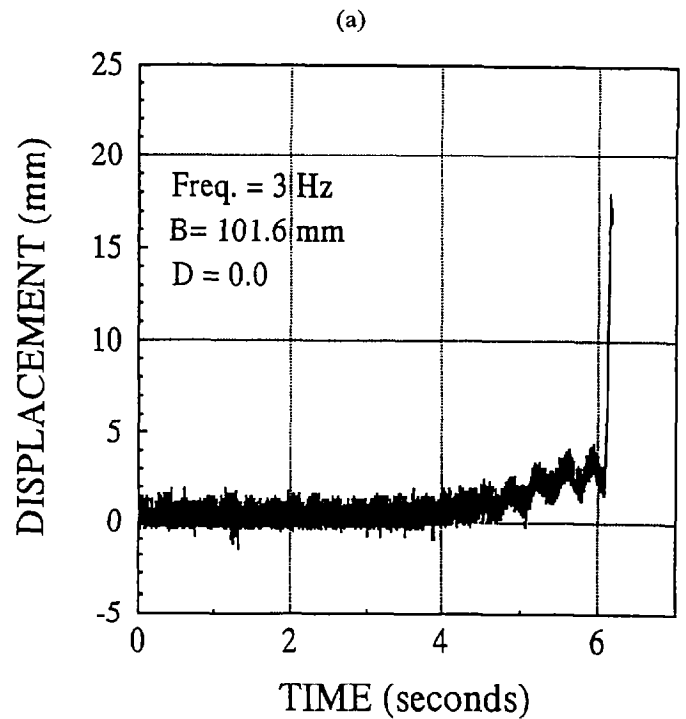
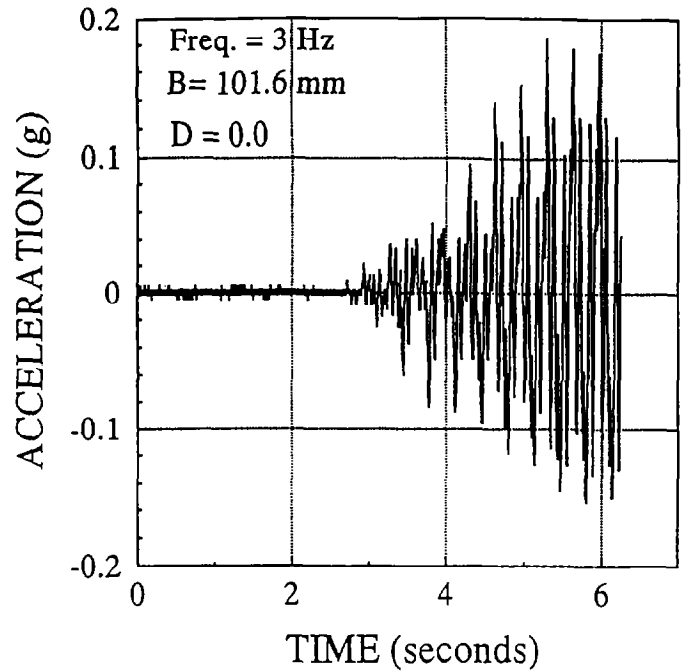


Fig. 7. Model S10F1 (a) variation of acceleration with time (b) variation of displacement with time.

determined from equation (I-10) in Appendix I. The theory predicts that failure would occur before the eccentricity reaches the values shown in Table 2.

Table 2. Comparison between the required horizontal acceleration ( $k_h$ ) for overturning and the theoretical critical acceleration ( $k_c$ ) for the model footings at two selected eccentricities.

Model footing	Eccentricity	$k_h$	$k_c$
S10F3	B/6	0.19	0.097
S10F1		0.09	0.0
S10F3	B/2	0.57	0.097
S10F1		0.28	0.0

### CRITICAL ACCELERATION

Model square footings with different values of safety factors were shaken at different levels of horizontal acceleration to determine the critical acceleration ( $k_c$ ). The critical acceleration was determined from the test results as the acceleration at which vertical movement and/or rotation of the footing was initiated. The results of the critical acceleration for models S10F1 and S10F3 are shown in column 2 of Table 3 and the rotations at different acceleration levels are shown in Fig. 9.

Table 3. Comparison between the critical accelerations of experiments and various seismic bearing capacity equations.

Footing	Critical acceleration			
	Experiment	Budhu & Richards Al-Karni (1993)	et. al. (1991)	Sarma & Iossifelis (1990)
S10F3	0.25	0.097	0.138	0.132
S10F1.2	0.14	0.017	0.022	0.018
S10F1	0.08	0.0	0.0	0.0

### FREQUENCY EFFECTS

Model footings were also tested at frequencies ranging from 1 Hz to 4 Hz in steps of 1 Hz. No significant differences among the seismic responses of the footings were observed at these frequencies.

### FOOTING SHAPE

Two different shapes of footings were tested to study the effects of footing shape on the seismic bearing capacity. One, a square footing of size 7.62cm x 7.62cm and the other a rectangular footing of size 7.62 cm x 11.43 cm were tested with static safety factors of one and three. Both footings were located on the top surface of the sand bed, i.e., they were tested as surface footings. The longer side of the rectangular footing was perpendicular to the direction of motion.

The critical acceleration determined from the experimental results was approximately the same for both shapes of footing. The rotations of the rectangular footing (Fig. 9) were higher than the rotations of the square footing for a safety factor of 1 but similar for a safety factor of 3.

### DEPTH OF EMBEDMENT

Model square footings (7.62cm x 7.62 cm) were constructed with safety factors ranging from 1 to 6.2 and embedment ratios ( $D_f/B$ ) of 0, 1/3 and 2/3. As the depth of embedment increases, the safety factor increases and the mass of an embedded footing required

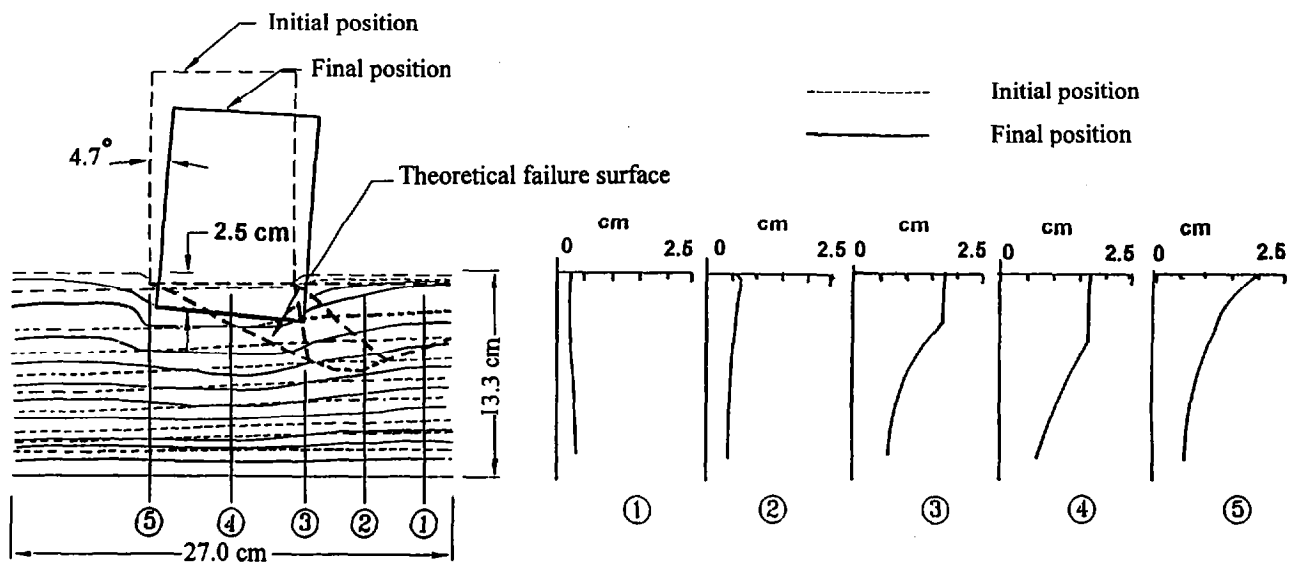


Fig. 8. Positions of lines of dust in the sand bed and the displacement of a model footing at an acceleration of 0.5 g. The figures on the right show the vertical profiles of the lines of dust in the sand bed at 0.5g.



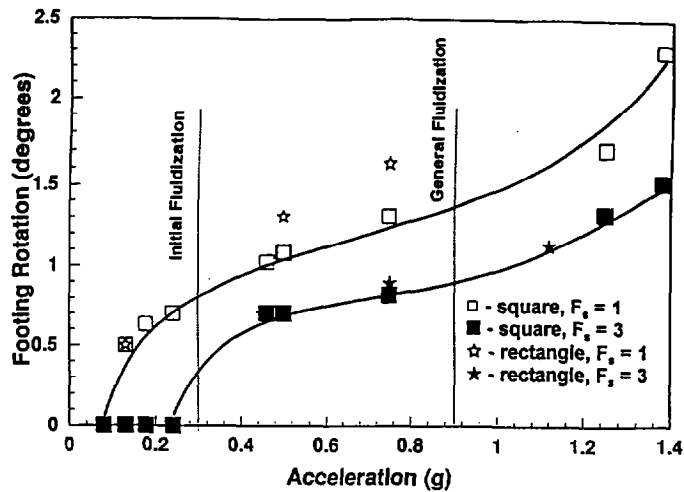


Fig. 9. Rotations of models footings at different values of peak acceleration.

to maintain a safety factor equivalent to a surface footing then increases. Thus, the embedded footings had greater heights than the surface footing because the cross sectional areas were the same. The measured rotations per unit height of footing at various safety factors for  $k_h = 0.5$ , frequency = 3 Hz and duration = 10 seconds are shown in Fig. 10. There seems to be no significant effect of the depth of embedment on the rotation of the footing.

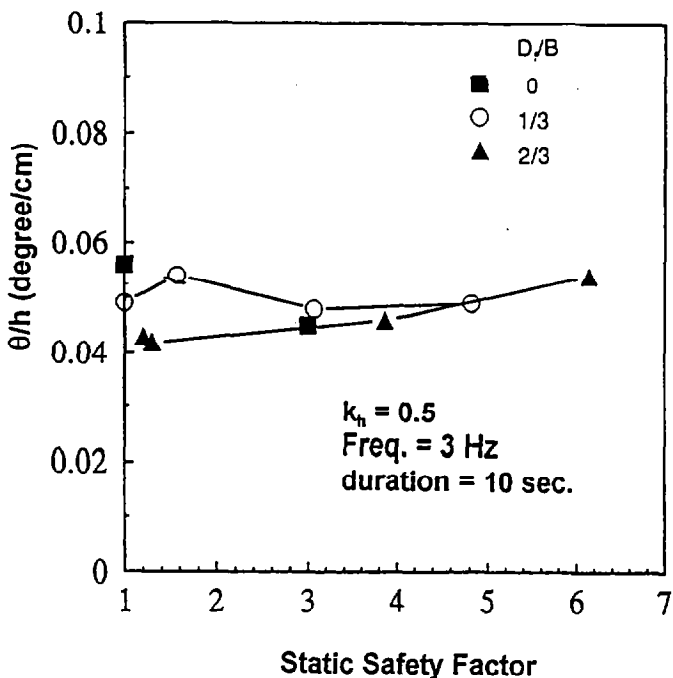


Fig. 10 Variation of footing rotation with safety factor for different embedment to width ratio.

## RELATIVE DENSITY

Model S10F1 was used to investigate the effects of relative density on the seismic bearing capacity. The results revealed no significant effect of relative density on the footing rotation. For example, for an acceleration regime consisting of an amplitude of 0.52g, frequency of 3 Hz and duration of 10 seconds, the footing rotations measured were 0.95° for a relative density of 41% and 1.06° for a relative density of 67%.

## DISCUSSION

The critical acceleration was determined when a sudden rotation of the footing occurred. At this acceleration, no failure plane or surface was detected in any of the tests conducted in this experimental program. Even if a failure surface was formed, our experimental method was too crude to detect it.

The theoretical critical acceleration can be determined from the proposed seismic bearing capacity equations by finding the acceleration for a safety factor of 1 (Appendix I). A comparison between the predictions of critical accelerations from the various proposed seismic bearing capacity equations and the experimental results is shown in Table 2. None of the predictions from the proposed bearing capacity equations using the initial angle of friction of the sand compares favorably with the measured critical acceleration determined from the experiments - all are much lower than the experimental results.

A critical acceleration of 0.08g was obtained from the experiments for a footing with a static safety factor of 1. This shows that either the static bearing capacity equations are conservative or the angle of friction of the soil used in computing the static bearing capacity is different from the test value. Zadroga (1994) reported that the static bearing capacity of cohesionless soils obtained from model footing experiments done in several laboratories were greater (some by as much as 100%) than computed values using static bearing capacity equations. The variation in relative density in forming a sand bed in the shake table with the spreader bar at a fixed setting was  $\pm 5\%$ . This leads to a change in of about  $\pm 2^\circ$  that can change the static bearing capacity significantly. For example, if  $\phi = 43^\circ$  rather than  $41^\circ$ , the static bearing capacity would increase by about 40%. Three similar tests on a square footing (7.62 cm x 7.62 cm) were conducted and the results revealed a maximum difference of about 25% in the critical acceleration. This is attributed to the differences between used in computing the weight of the models and in the actual test.

For model footing (S10F1.2) an average settlement of about 1.8 cm ( $S/B = 10\%$ , where  $S$  is the settlement, and  $B$  the footing width) occurred just under the footing. This settlement is a combination of soil densification and fluidization settlement. The average densification settlement was about 1 cm and was concentrated over a depth of about  $4B$ . The average vertical strain over this region is then about 2.5% and resulted in a significant change in the angle of friction. With an initial void ratio of 0.7, the relative density changed from 67% to 79% resulting in an increase of the angle of friction of  $4^\circ$  (Fig. 3). The static bearing capacity factor increases from  $N_{\gamma} = 130$  ( $\phi = 41^\circ$ ) to 272 ( $\phi = 45^\circ$ ) which produces a static factor of safety of 2.4 rather than 1.2 for model S10F1.2. Solving equation I-8 (Appendix I) for an  $F_s = 2.4$ , gives  $k_c = 0.077$ . There are reasonable predictions and establish that cyclic densification during a seismic event can significantly increase the critical acceleration. The predictions of Richards et. al. (1991) are remarkably close to the experimental results and it is possible that the failure mechanism they assumed best represent the actual failure mechanism in the model tests compared with the other investigators mentioned in Table 3. However this is difficult to ascertain since the authors did not observe any distinct failure surface in the experiments.

A comparison of the failure surface assumed by Budhu and Al-karni (1993) in their analysis and the observed displacement profile under a model footing is shown in Fig. 8. Although the determination of the failure surface from the experiments is unreliable, the experimental results do provide a rough estimate of the form of the seismic failure surface. The displacement patterns under the footing are asymmetrical as expected but they are unlike the shapes of theoretical slip surfaces assumed in analyses of seismic bearing capacity. Making a valid judgement on the form of the failure surface is difficult since the measurement method used here is rather crude.

Richards et. al. (1990) showed, from a free-field solution, that slip planes will be initiated in a dry sand when

$$\frac{k_h^*}{1 - k_v^*} = \frac{\sin \phi}{2} [(\sin \phi - 3)(\sin \phi - 1)]^{0.5} \quad (11)$$

where  $k_h^*$  and  $k_v^*$  are the horizontal and vertical acceleration coefficients respectively when the slip planes are initiated. Richards et. al. (1990) called this stage initial shear fluidization. They further showed that a state of general shear fluidization existed when the horizontal acceleration is

$$(k_h) = \tan \phi \quad (12)$$

for  $k_v = 0$ . At general shear fluidization, the soil mass is expected to behave like a viscous fluid. This general fluidization is different from liquefaction caused by excess pore water pressure generation during seismic loading. General shear fluidization is the temporary change of state of a soil mass from a solid-like material to a viscous-fluid like material when the acceleration exceeds that given by equation (12).

Equations (11) and (12) set bounds for the critical accelerations of shallow footings. The acceleration required to initiate slip planes (initial shear fluidization) in the soil provides an upper limit to the critical acceleration for shallow footings. Regardless of the safety factor used, the critical acceleration must be less than or equal to the initial shear fluidization acceleration. For  $\phi = 41^\circ$  and  $k_v^* = 0$ , equations (11 and 12) give  $k_h^* = 0.294$  and  $(k_h)_f = 0.87$  and, therefore, the critical acceleration for the footings must be less than 0.294g. An inspection of Table 2 and Fig. 9 shows that the critical acceleration of the footings obtained from the experiments are lower than  $k_h^*$ . Indeed, the critical acceleration for model footing S10F3 of 0.25g is very close to the initial shear fluidization acceleration (0.294g).

The theoretical general shear fluidization acceleration approximately marks the points of inflection of the rotation - acceleration curves shown in Fig. 9. Beyond the general shear fluidization acceleration, the footing will respond as a mass in a viscous fluid subjected to an acceleration field. The settlement and rotation of a footing will then depend on the viscosity of the sand and the frictional drag on the footing.

## CONCLUSIONS

The results of an experimental program to investigate the seismic bearing capacity of model shallow footings on a dry sand were presented in this paper. The results showed that the predictions of critical accelerations from recently proposed seismic bearing capacity equations are conservative when compared with the experimental results. The disagreement between the theoretical predictions and the experimental results stems from cyclic densification which significantly increased the angle of friction of the soil and the experimental difficulties in obtaining the desired angle of friction of the soil in the test setup. When corrections were made to allow for changes in angle of friction caused by cyclic densification, it was found that the Richards et. al. (1991) equation gave the best prediction of the critical acceleration. The displacement profile under a model footing, obtained from rather unsophisticated methods and interpreted as symbolic of a failure surface, did not match failure surfaces assumed in theoretical analyses. The initial shear fluidization

acceleration of the soil mass defines an upper limit for critical acceleration for shallow footings on sands. Irrespective of the static bearing capacity safety factor, the critical acceleration cannot exceed the acceleration to cause initial shear fluidization. Frequencies within the range 1 - 4Hz, relative densities within the range 40 - 70%, and footing shape (aspect ratio 1 - 1.5) did not significantly influence the rotations of the model footings.

## REFERENCES

- Al-Karni, A.A. [1993]. "Seismic Settlement and bearing capacity of Shallow Footings on cohesionless soil.", Ph.D. Dissertation, University of Arizona, Tucson, USA.
- Budhu, M., and Al-Karni, A. A. (1993). "Seismic bearing capacity of soils." *Geotechnique*, 43 (1), pp. 181-187.
- D'Appolonia, D.J., D'Appolonia, E.D. and Brissette, R.F. [1968]. "Settlement of spread footings on sand.", *J. SM & Fnds. Div., ASCE*, 94, pp. 1011-1053.
- Hansen, J. B. [1970]. "A revised and extended formula for bearing capacity.", Danish Geotechnical Institute, Bulletin 28, Copenhagen.
- Iai, S., [1989]. "Similitude for shaking table tests on soil-structure-fluid model in 1g gravitational Field.", *Soils and Foundations, JSSMFE*, 29 (1), pp. 105-118.
- Meyerhof, G. C., [1963]. "Some recent research on the bearing capacity of foundations.", *Canadian Geotechnical Journal*, 1 (1), pp. 16-26.
- Okamoto, S., [1984]. "*Introduction to earthquake engineering.*" University of Tokyo Press, Japan.
- Okamoto, S., [1956]. "Bearing capacity of sandy soil and lateral earth pressure during earthquakes.", *Proc. First World Conf. on Earthquake Eng., Berkeley, CA, Paper No.27.*
- Richards, R., Elms, D.G., and Budhu, M., [1990]. "Dynamic fluidization of soils.", *J. Geotech. Engrg., ASCE*, 116 (5), pp. 740-759.
- Richards, R., Elms, D.G., and Budhu, M. [1991]. "Soil fluidization and foundation behavior.", *Proc. Second International Conference on Recent Advances in Geotechnical Earthquake Engineering and Soil Dynamics, Rolla, Missouri, I*, pp. 719-723.
- Richards, R., Elms, D.G., and Budhu, M. [1993]. "Seismic bearing capacity and settlement of foundations.", *J. Geotech. Engrg.*, 119 (4), ASCE, pp. 662-674.
- Sarma, S. K., and Iossifelis, I. S. [1990]. "Seismic bearing capacity factors of shallow strip footings." *Geotechnique*, 40 (2), pp. 265-273.
- Seed, H. B., and Lee, K. L. [1966]. "Liquefaction of saturated sands during cyclic loading.", *J. Soil Mech. & Fnds. Engrg., ASCE* 92(SM6), pp. 105-134.
- Selig, E. T., and McKee, K. E. [1961]. "Static and dynamic behavior of small footings.", *J. Soil Mech. & Fnds. Engrg., ASCE.*, 87 (6), pp. 29-47.
- Terzaghi, K., [1943]. "*Theoretical Soil Mechanics.*" Wiley, New York.
- Vesic, A. S., Banks, D. C., and Woodard, J. M. [1965]. "An experimental study of dynamic bearing capacity of footing on sand.", *Proceeding, 6th International Conference on Soil Mechanics and Foundation Engineering, Montreal, Canada, 2*, pp. 209-213.
- Vesic, A.S. [1973]. "Analysis of ultimate loads of shallow foundation.", *J. Geotech. Engrg., ASCE*, 99 (1), pp. 43-73.
- Watanabe, T. [1966]. "Damage to oil refinery plants and a building on compacted ground by the Niigata earthquake and their restoration.", *Soils and Foundations, JSSMFE*, VI (2), pp. 86-99.
- Zadroga, B. [1994]. "Bearing capacity of shallow foundations on noncohesive soils.", *J. Geotech. Engrg., ASCE*, 120(11), pp. 1991-2008.

## APPENDIX I

The maximum stress,  $\sigma'_{max}$ , under a uniform square footing of width, B, and height, h, subjected to only a horizontal acceleration  $k_h g$  (Fig. I-1) is

$$\sigma_{max} = \frac{W}{B^2} \left( 1 + \sigma k_h \frac{\bar{h}}{B} \right) \quad (I-1)$$

where  $\bar{h}$  is the distance from the center of mass to the bottom of the footing. For a footing of uniform height, Equation (I-1)

$$\sigma_{max} = \frac{W}{B^2} \left( 1 + 3 k_h \frac{h}{B} \right) = \sigma_s \left( 1 + 3 k_h \frac{h}{B} \right) \quad (I-2)$$

where W is the weight of the footing, and  $\sigma_s$  is the

allowable static vertical stress. Now

$$\sigma_s = \frac{q_{uS}}{F_s} \quad (I-3)$$

and

$$\sigma_{max} = \frac{q_{uE}}{F_E} \quad (I-4)$$

where  $q_{uS}$  and  $q_{uE}$  are the static and seismic ultimate bearing capacity, and  $F_s$  and  $F_E$  are the safety factors for static and seismic loads respectively. Substituting equations (I-3) and (I-4) into equation (I-2), we obtain

$$\frac{q_{uE}}{F_E} = \frac{q_{uS}}{F_s} \left( 1 + 3k_h \frac{h}{B} \right) \quad (I-5)$$

For a surface footing on a cohesionless soil, the ultimate seismic bearing capacity from equation (1) is

$$q_{uE} = q_{uS} e_\gamma = q_{uS} \exp(-9k^{1.1}) \quad (I-6)$$

Substituting equation (I-6) into equation (I-5), we obtain

$$\frac{\exp(-9k_h^{1.1})}{F_E} = \frac{1}{F_s} \left( 1 + 3k_h \frac{h}{B} \right) \quad (I-7)$$

The critical acceleration at failure is found by substituting  $F_E = 1$  and  $k_h = k_c$  in equation (I-7), giving

$$\exp(-9k_c^{1.1}) = \frac{1}{F_s} \left( 1 + 3k_c \frac{h}{B} \right) \quad (I-8)$$

The critical acceleration ( $k_c$ ) can be determined by solving equation (I-8). For S10F3,  $b = 10.16\text{cm}$ ,  $F_s = 3$ , and  $h = 17.8\text{ cm}$ , the critical acceleration  $k_c = 0.097g$ .

From the analysis of Richards et. al. (1993) equation (I-8) is,

$$\exp(-3.3k_c^{0.9}) = \frac{1}{F_s} \left( 1 + 3k_c \frac{h}{B} \right) \quad (I-9)$$

and from the analysis of Sarma and Iossifelis (1990) equation (I-8) is,

$$\exp(-8k_c^{1.3}) = \frac{1}{F_s} \left( 1 + 3k_c \frac{h}{B} \right) \quad (I-10)$$

A comparison of the critical accelerations computed using the above analysis for the model footings S10F1 and S10F3 are shown in Table 3.

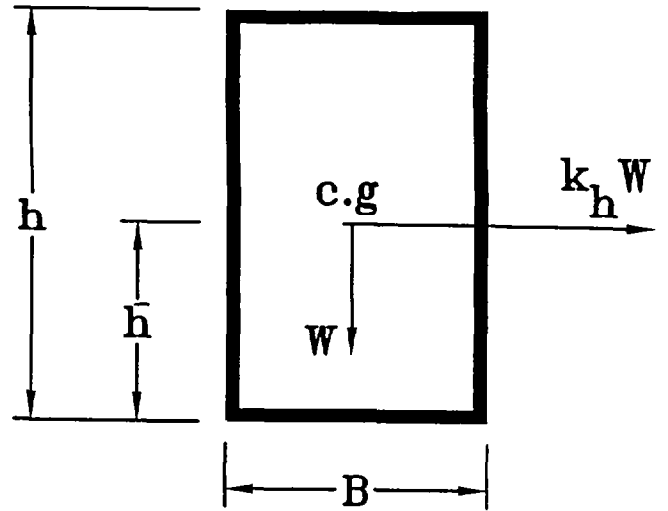


Fig. I.1. A square footing subjected to a horizontal acceleration.

#### NOTATIONS

- B footing width.
- C soil cohesion parameter.
- $d_c$ ,  $d_q$ , and  $d_r$  bearing capacity depth factors.
- $D = C/\gamma H$ , stability factor.
- $D_f$  depth of footing
- $e_c$ ,  $e_q$ , and  $e_\gamma$  bearing capacity seismic factors.
- $F_s$  static safety factor.
- h footing height.
- H depth of failure zone.
- $k_h$ , &  $k_v$  horizontal and vertical acceleration coefficients.
- $k_c$  critical acceleration coefficient.
- $k_h^*$  initial fluidization acceleration coefficient.
- $(k_h)_f$  general fluidization acceleration coefficient.
- $N_{cS}$ ,  $N_{qS}$ , &  $N_{\gamma S}$  static bearing capacity factors.
- $N_{cE}$ ,  $N_{qE}$ , &  $N_{\gamma E}$  seismic bearing capacity factors.
- $q_f$  overburden pressure.
- $q_{uE}$  ultimate seismic bearing capacity.
- $q_{uS}$  ultimate static bearing capacity.
- Q ultimate load.
- $s_c$ ,  $s_q$ , and  $s_\gamma$  bearing capacity shape factors.
- $\phi$  angle of internal friction of the soil.
- $\gamma$  soil density.
- $\lambda$  scale factor.
- $\sigma_{max}$  maximum vertical stress.
- $\sigma_s$  allowable static vertical stress.